Bipyridine-containing Host Materials for High Performance Yellow Thermally Activated Delayed Fluorescence-based Organic Light Emitting Diodes with Very Low Efficiency Roll-Off

Dongyang Chen,[a] Pachaiyappan Rajamalli,[a] Francisco Tenopala-Carmona,[b] Cameron L. Carpenter-Warren,[a] David B. Cordes,[a] Changmin Keum,[b] Alexandra M. Z. Slawin,[a] Malte Gather,[b] and Eli Zysman-Colman[a]

[a] Organic Semiconductor Centre, EaStCHEM School of Chemistry, University of St Andrews, St Andrews, Fife, UK, KY16 9ST, Fax: +44-1334 463808; Tel: +44-1334 463826; E-mail: eli.zysman-colman@st-andrews.ac.uk;

[b] Organic Semiconductor Centre, SUPA School of Physics and Astronomy, University of St Andrews, St Andrews, Fife, UK, KY16 9SS

Abstract

Two bipolar host materials **3-CBPy** and **4-mCBPy** are reported. These hosts are structural analogs of the common host materials CBP and mCBP wherein the phenyl rings have been replaced with pyridines. The two materials possess deep HOMO and shallow LUMO levels along with sufficiently high energy S_1 and T_1 states that make them suitable hosts for yellow emitters in electroluminescent devices. Yellow-emitting thermally activated delayed fluorescence (TADF) organic light-emitting diodes (OLEDs) were fabricated using 2,4,6-tris(4-(10H-phenoxazin-10-yl)phenyl)-1,3,5-triazine (tri-PXZ-TRZ) as the dopant emitter with either **3-CBPy** or **4-mCBPy** employed as the host. Their

device performance was compared to analogous devices using CBP and mCBP as host materials. The pyridine-containing host devices showed markedly improved external quantum efficiencies (EQE) and decreased roll-off. The 7 wt% tri-PXZ-TRZ-doped device exhibited very low turn-on voltage (2.5 V for both **3-CBPy** and **4-mCBPy**) along with maximum external quantum efficiencies (EQE_{max}) reaching 15.6% (for **3-CBPy**) and 19.4% (for **4-mCBPy**). The device using **4-mCBPy** also exhibited very low efficiency roll-off with an EQE of 16.0% at a luminance of 10,000 cd m^{-2}.

Introduction

Materials development related to organic light-emitting diodes (OLEDs) has accelerated significantly since Adachi and co-workers demonstrated high efficiency devices employing all organic thermally activated delayed fluorescence (TADF) emitters in 2012.[1] TADF emitters can harvest singlet excitons and triplet excitons simultaneously resulting in a theoretical maximum internal quantum efficiency (IQE) of 100% and very attractive external quantum efficiency (EQE).[2] In the past seven years there have been hundreds of TADF emitters reported, most of which based on a donor-phenyl bridge-acceptor design paradigm.[1, 3] As TADF emitters usually have long emission lifetimes originating from triplet excitons, OLED efficiency, stability and efficiency roll-off can all be adversely affected by a range of deactivation mechanisms including: triplet-triplet annihilation (TTA), triplet-polaron quenching (TPQ), and singlet-triplet annihilation (STA).[4] To avoid concentration quenching the most common solution is to dope the emitter into an appropriate host. For TADF emitters that are themselves ambipolar, an ambipolar host can both tune the emission wavelength and improve the device performance by narrowing singlet-triplet energy gap (ΔE_{ST}) and thereby boosting the reverse intersystem crossing (rISC) rate, k_{rISC}.[5] However,

currently most host materials used for TADF emitters are inherited from those used in phosphorescent OLEDs, which are mainly unipolar materials.[6] The TADF OLEDs based on traditional hosts usually exhibit high turn-on voltages and severe efficiency roll-off.[1b, 7] To address these issues, several ambipolar host materials have been designed and employed in TADF based OLEDs.[5b, 8]

The first sky-blue TADF OLED, reported in 2012, used PPT as host and **2CzPN** as emitter. The maximum EQE value (EQE_{max}) reached for this OLED was only 8% at a current density of 5×10^{-4} mA cm^{-2}, with λ_{EL} of 470 nm.[1a] Zhang *et al.*[8a] designed an ambipolar host, ***m*-CzCN**, possessing a cyano-substituted phenyl as the n-type unit and an *N*-phenyl-substituted carbazole as the p-type unit. This host shows deep blue emission in the neat thin film with λ_{PL} at 403 nm and high energy singlet (S_1) (3.48 eV) and triplet (T_1) (2.81 eV) states that match well the absorption of **2CzPN**, which permits efficient Förster resonant energy transfer (FRET) to confine the exciton on the emitter. The host also exhibited preferable hole and electron mobilities (1.35×10^{-6} cm^2 V^{-1} s^{-1} and 2.40×10^{-7} cm^2 V^{-1} s^{-1}, respectively). As a result, the OLEDs based on **2CzPN/*m*-CzCN** exhibited a much higher EQE_{max} = 15% (at a luminance of 100 cd m^{-2}) with CIE (0.17, 0.26). This efficiency record was soon surpassed as Choi *et al.*[8b] who reported another ambipolar host **ZDN** for **2CzPN** that contains a carbazole p-type unit and a pyridoindole n-type unit, both attached to a dibenzothiophene. The polar host stabilizes the S_1 state of **2CzPN** resulting in an increased k_{rISC}. The device based on **2CzPN/ZDN** exhibited an outstanding EQE_{max} of 25.7% (at a luminance of 45 cd m^{-2}). However, the electroluminescence was red-shifted from (0.16, 0.30) in **mCP** to (0.19, 0.39) in **ZDN** and showed strong efficiency roll-off, with EQE at 1000 cd m^{-2} (EQE_{1000}) = 6%.[8c] To

address the issue of efficiency roll-off, Cheng *et al*.[5b] designed an ambipolar TADF host **BT-01**, which contains carbazole as the n-type unit and diphenylsulfone as the p-type unit. The host has a ΔE_{ST} of 0.35 eV that is sufficiently small to allow the triplet excitons to upconvert to singlet excitons via rISC. These singlet excitons are then transferred to the TADF emitter via FRET process. The high polarity of this host contributes to an increased TADF quantum efficiency (Φ_{TADF} = 53%) and faster k_{rISC} of 1.6×10^4 s^{-1} for **2CzPN**, both of which are higher than those in mCP host (Φ_{TADF} = 38%, k_{rISC} = 6.7×10^3 s^{-1}). As a result of these attributes, the OLED based on **2CzPN/BT-01** shows an excellent EQE_{max} of 25.2% (at a luminance of 8 cd cm^{-2}) with CIE of (0.16, 0.31), and further shows improved efficiency roll-off with EQE_{1000} = 10%. These metrics place this device amongst the best for **2CzPN**-based OLEDs and demonstrate that with a suitable host, the efficiency of TADF-based OLEDs can be boosted significantly while maintaining very low efficiency roll-off. Despite the potential of suitably designed hosts, there is a dearth of reports for appropriate hosts for yellow to red TADF emitters.[8d, 8e]

An ideal host material for yellow-to-red TADF yellow emitters should have: (1) sufficiently high singlet and triplet state energies for exciton confinement; (2) appropriate HOMO and LUMO levels to avoid charge trapping on the emitter and to facilitate charge transport through the device; (3) broad spectral overlap with the emitters for efficient Förster energy transfer; and (4) ambipolar character to facilitate charge transport and carrier injection.[9] To satisfy these requirements, the choice of building segments and the connectivity of the host should be carefully considered. The pyridine and bipyridine moieties have been used within electron-transporting materials, and there are a few reports of their use as bipolar hosts[10] due to their electron-transporting ability, while

carbazole is commonly employed as a hole-transporting unit in the design of high-energy hosts.[11] The combination of bipyridine with carbazole should produce an ambipolar host with desirable charge transporting properties. In this work, we report bipyridine analogs of the two commonly used commercial hosts 3,3-di(9H-carbazol-9-yl)biphenyl (**mCBP**) and 4,4'-bis(*N*-carbazolyl)-1,1'-biphenyl (**CBP**). The two new hosts are 4,4'-di(9H-carbazol-9-yl)-2,2'-bipyridine (**4-mCBPy**) and 6,6'-di(9H-carbazol-9-yl)-3,3'-bipyridine (**3-CBPy**), both of which were readily synthesized in one or two steps. Both materials possess high S_1 energies around 3.3 eV and T_1 energies around 2.7 eV and have deep HOMO (-5.75/-5.80 eV for **3-CBPy**/**4-mCBPy**) and shallow LUMO levels (-2.59/-2.70 eV for **3-CBPy**/**4-mCBPy**). All four materials were assessed as hosts in yellow TADF OLEDs using the previously reported **tri-PXZ-TRZ** as the emitter.[12] In the original report on **tri-PXZ-TRZ** in 2013, **mCBP** was used as host material and the device exhibited an EQE_{max} of 13.4%.[12] Very recently, Meng *et al.* utilized **CBP** as host with optimized device structure and improved the EQE_{max} to 21%.[13] In the present work the devices employing **4-mCBPy** and **3-CBPy** as hosts showed much improved external quantum efficiencies, very low efficiency roll-off and turn-on voltages compared to analogous devices using **mCBP** and **CBP** as host materials.

Examples of bespoke hosts for 2CzPN

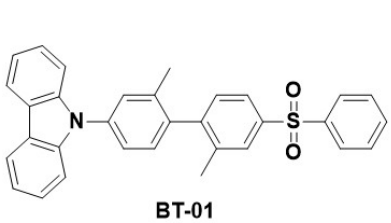

BT-01
Chem. Mater. **2017,** *29,* 1527-1537.

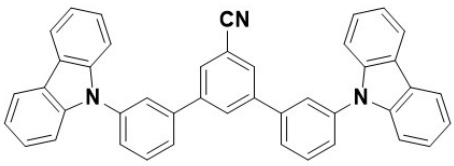

m-CzCN
J. Mater. Chem. C **2015,** *3,* 12529-12538.

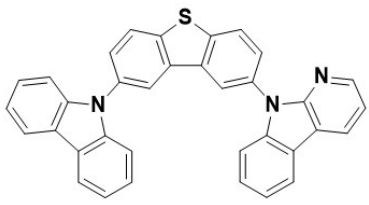

ZDN
J. Mater. Chem. C **2016,** *4,* 4512-4520.

Present work

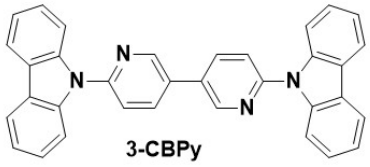

3-CBPy

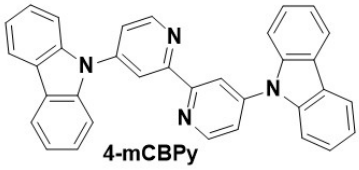

4-mCBPy

Figure **1.** The structures of bespoke hosts and hosts in this work

Results and Discussion

Synthesis and Chemical Characterization

The two bipyridine-based hosts were easily obtained in high yields (Scheme **1**). For **3-CBPy**, 5-bromo-2-iodopyridine was first reacted with carbazole in a copper-promoted Ullman reaction to afford 9-(5-bromopyridin-2-yl)-9H-carbazole in excellent yield.[14] This intermediate was homocoupled, catalyzed by an *in situ*-formed nickel(0) species to obtain **3-CBPy** in 72% over the two steps. The host **4-mCBPy** was prepared by copper-promoted Ullman reaction between 4,4'-dibromo-2,2'-bipyridine and excess carbazole.[14] Both syntheses of **3-CBPy** and **4-mCBPy** have been conducted on gram scale without loss of yield. The identity and purity of both compounds were ascertained using a combination of ^{1}HNMR and ^{13}CNMR spectroscopy, high resolution mass spectrometry, high performance liquid chromatography, and elemental analysis. Crystals of **3-CBPy** suitable for single crystal X-ray diffraction were obtained from a mixed solution of toluene and hexane while crystals of **4-mCBPy** were obtained by thermal sublimation. The bipyridine moiety in both **3-CBPy** and **4-mCBPy** exhibited a planar *trans* conformation (torsion angles of 1.44(11)° and 0°, respectively) while the torsion angles between the bipyridine and carbazoles were 36.54(12)° and 39.84(11)° (**3-CBPy**), and 39.55(11)°, respectively. The angles between pyridyl rings and those adjacent are maintained by CH···N hydrogen bonds with H···N distances of 2.58 – 2.65 Å and 2.46 Å for **3-CBPy** and **4-CBPy**, respectively [C···N separations for **3-CBPy** of 3.0312(16) – 3.0998(17) Å and for **4-CBPy** of 2.7876(15) Å]. Only **3-CBPy** shows significant intermolecular interactions, with both π···π interactions between adjacent carbazoles at a centroid···centroid distance of

3.4949(8) Å, and CH···π interactions between pyridyl hydrogens and both carbazole and pyridyl π-systems at H···centroid separations of 2.63-2.93 Å and corresponding C···centroid separations of 3.1417(12)–3.6066(12) Å. These distances are close to the conventional van der Waals limit, but CH···π interactions have been suggested to be effective at distances beyond this limit.[15] No equivalent interactions are seen in **4-mCBPy**, the shortest centroid···centroid distance being 3.9506(10) Å and shortest CH···centroid separation being 3.53 Å. The interactions in **3-CBPy** give rise to sheets lying in the crystallographic *bc*-plane.

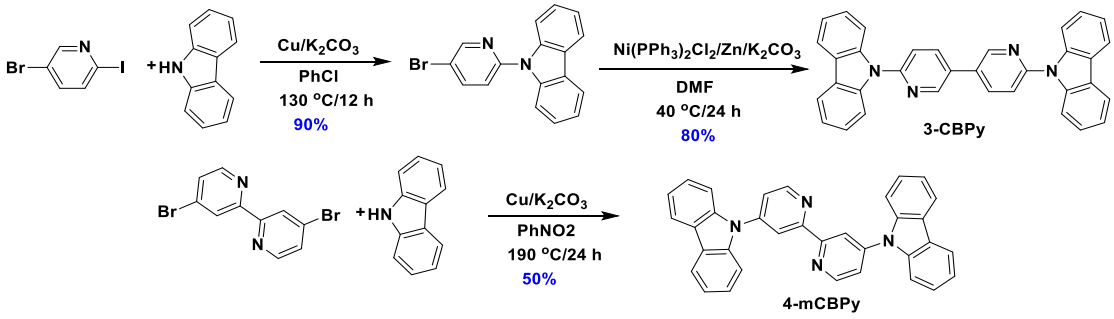

Scheme **1**. Synthesis of **3-CBPy** and **4-mCBPy**

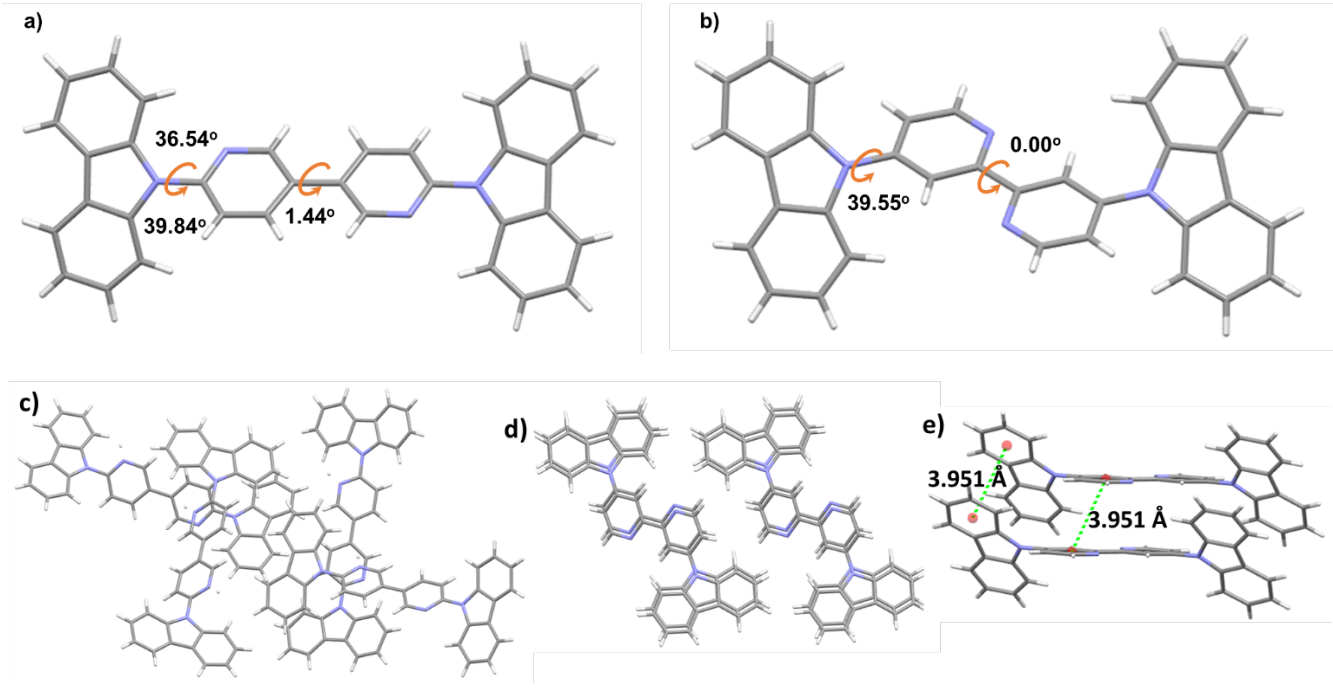

Figure **2.** Single crystal structure of (a) **3-CBPy** and (b) **4-mCBPy** (c) packing mode of **3-CBPy**, (d) packing mode of **4-mCBPy**, and (e) packing distance of **4-mCBPy**. Minor components of

disorder are omitted for clarity.

The two hosts exhibited high melting (T_m) and thermal degradation temperatures (T_d) (defined as temperature at 5% weight loss) as assessed by thermogravimetric analysis (TGA) and differential thermal analysis (DTA), Figure **S11**. The T_m for **3-CBPy** and **4-mCBPy** were 310 °C and 320 °C, which are higher than the T_m of CBP (283 °C) and mCBP (271 °C).[16] The two hosts also exhibited superior thermal stability with no weight loss observed up to 350°C and a T_d for **3-CBPy** and **4-mCBPy** of 388 °C and 382 °C, respectively. The T_d values of the two new hosts are thus higher than both CBP (365 °C) and mCBP (315 °C).[16] The superior thermal stabilities of **3-CBPy** and **4-mCBPy** would (1) guarantee that these materials can be thermally sublimed and (2) support device stability at high driving voltage and high brightness.

Theoretical Calculations

Density functional theory (DFT) and time-dependent DFT (TDDFT) calculations of **3-CBPy** and **4-mCBPy** using PBE0/6-31G(d, p) in the gas phase were undertaken to evaluate *in silico* their HOMO/LUMO and singlet/triplet state energies.[17] The results are summarized in Figure **3**. The modelling indicates that **4-mCBPy** possesses a slightly larger HOMO-LUMO gap than **3-CBPy** but that the frontier orbitals in the former are much more spatially separated, leading to a reduced exchange integral and a significantly smaller singlet-triplet energy gap compared to **mCBP** and **CBP**. In both hosts, the HOMO is mainly distributed on the carbazole moieties while the LUMO is localized on the bipyridine core. The HOMO of **3-CBPy**, however, is distributed across the entire molecule due to its more planar conformation in the gas phase. The increased conjugation present

in **3-CBPy** leads to an increased HOMO energy of -5.66 eV compared to that in **4-mCBPy** at -5.83 eV. The trend in LUMO energies of **3-CBPy** and **4-mCBPy** are similar with values of -1.41 eV and -1.56 eV, respectively. TDDFT calculations reveal that the S_1 energies are essentially identical at ca. 3.60 eV for the two hosts, but that the T_1 energy of **3-CBPy** is more stabilized at 3.06 eV compared to that of **4-mCBPy** (3.28 eV). The HOMO and LUMO levels of **3-CBPy** are slightly stabilized with respect to **CBP**, owing to the presence of the electron-withdrawing bipyridine core in the former. Both the S_1 and T_1 energies of **3-CBPy** are stabilized compared to **CBP** while ΔE_{ST} is only slightly reduced. The comparison, however, is starker when comparing **4-mCBPy** to **mCBP**. The HOMO of **4-mCBPy** is stabilized by 0.17 eV while the LUMO is stabilized by 0.47 eV compared to **mCBP**, which leads to a markedly reduced HOMO-LUMO gap of 4.27 eV for **4-mCBPy** compared to 4.57 eV for **mCBP**. The S_1 and T_1 states are likewise significantly stabilized in **4-mCBPy** compared to **mCBP**.

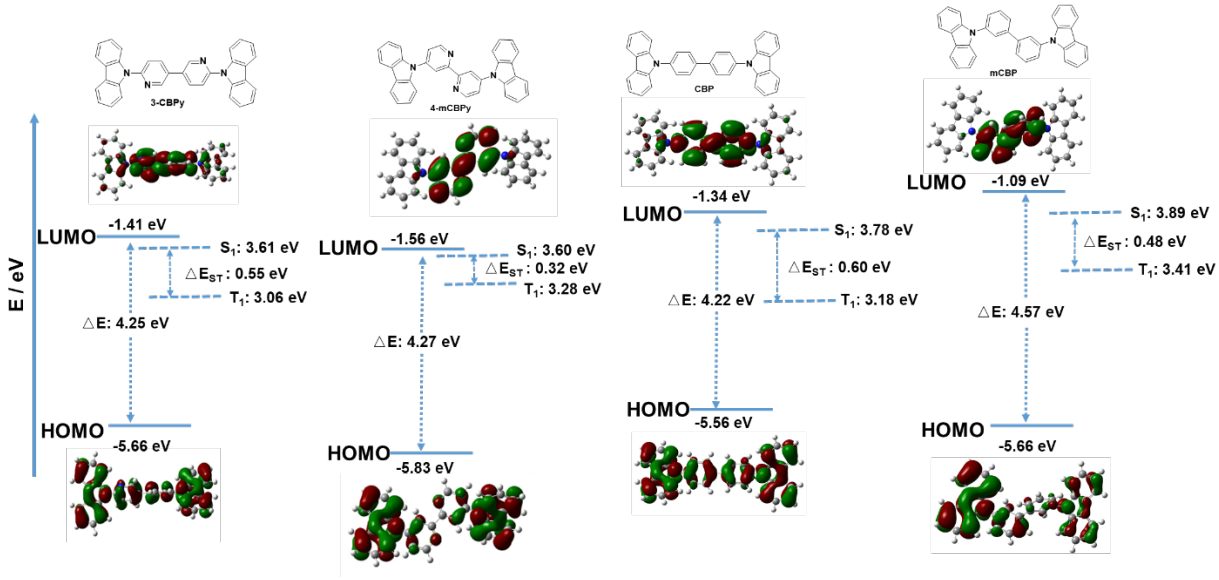

Figure **3**. Theoretical modelling of the energies of the HOMO/LUMO orbitals and the S_1 and T_1 states of **3-CBPy** and **4-mCBPy** and the electron density distribution of the frontier molecular orbitals.

Electrochemistry

The electrochemical properties of the two new hosts were analyzed by cyclic voltammetry (CV) and differential pulse voltammetry (DPV) measurements using 0.1 M tetra(*n*-butyl)ammonium hexafluorophosphate (*n*-Bu_4NPF_6) as the supporting electrolyte in degassed *N,N*-dimethylformamide (DMF). Voltammograms are referenced versus Fc/Fc^+ and the data reported versus a saturated calomel electrode (SCE). As shown in Figure **4**, **3-CBPy** and **4-mCPy** have distinct irreversible oxidation and reduction waves, which are assigned to the oxidation of carbazole and reduction of the bipyridine moieties, respectively, based on the DFT analysis. **3-CBPy** exhibited a slightly more negative reduction potential (E_{pc}^{red} = -1.66 V) than **4-mCBPy** (E_{pc}^{red} = -1.51 V), which indicates that 3,3'-bipyridyl possesses slightly weaker electron-withdrawing character than 4,4'-bipyridyl, conclusions in line with the DFT calculations. **4-mCBPy** shows a more stabilized oxidation (E_{pa}^{ox} = 1.55 V) than **3-CBPy** (E_{pa}^{ox} = 1.50 V), which is a function of the increased conjugation in the latter. The DPV scans show that both oxidation and reduction processes are mono-electronic in nature. The corresponding HOMO levels of **3-CBPy** and **4-mCBPy** were calculated to be -5.75 eV and -5.80 eV while the LUMO levels of **3-CBPy** and **4-mCBPy** were calculated to be -2.59 eV and -2.70 eV, respectively. The corresponding HOMO-LUMO gaps for **3-CBPy** and **4-mCBPy** are 3.16 eV and 3.10 eV, respectively. The HOMO/LUMO values of **3-CBPy** and **4-mCBPy** are comparable to the HOMO/LUMO values of **CBP** (-2.60 eV/-5.91 eV) and **mCBP** (-2.44 eV/-5.95 eV), and the trend in HOMO/LUMO values also broadly matched the DFT calculation.[18]

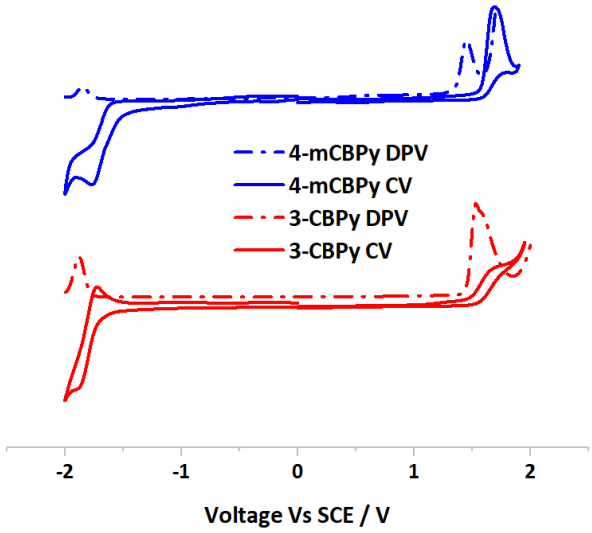

Figure **4**. Cyclic Voltammograms (CV, solid lines) and Differential Pulse Voltammograms (DPV, dashed lines) for **3-CBPy** and **4-mCBPy** in degassed DMF solution containing *n*-NBu_4PF_6 as the supporting electrolyte and using Fc/Fc^+ as an internal standard (Fc/Fc^+ = 0.55 eV versus SCE).[19]

Photophysics

The absorption and emission spectra of the two hosts in PhMe are shown in Figure **5a**. Both hosts exhibited strong absorption bands at around 290 nm, which are assigned to π-π* transitions, and absorption bands in the range 330-350 nm. These low energy bands are assigned based on TDDFT calculations as hybrid charge-transfer and π-π* transitions (Figure **S12**). The optical gap energies (E_{opt}), determined from the intersection point of the normalized absorption and emission spectra, are 3.35 eV for **3-CBPy**, and 3.49 eV for **4-mCBPy**, respectively. The photoluminescence spectrum of **3-CBPy** shows a narrow and sharp profile with a maximum of 384 nm while that of **4-mCBPy** is slightly red-shifted at 392 nm and broader. The unstructured character of both spectra is an indication of emission from a charge-transfer state. The emission spectra of both hosts were found to perfectly overlap with the absorption spectrum of the yellow TADF emitter **tri-PXZ-TRZ**,

indicating that efficient FRET is feasible. The photoluminescence quantum yields (Φ_{PL}) of **3-CBPy** and **4-mCBPy** were measured to be 23% and 17%, respectively, in degassed toluene solution and the emission lifetimes, (τ_{PL}) were 1.9 ns and 3.9 ns, respectively (Figure **S12**), indicating that both compounds are fluorescent in nature. The Φ_{PL} of spin-coated neat films of **3-CBPy** and **4-mCBPy** under a nitrogen atmosphere are 9% and 6%, respectively. The 77 K prompt fluorescence and phosphorescence spectra of neat films of the two hosts were measured to determine the S_1 and T_1 energies (Figure **5b** and **5c**). The S_1 energies of **3-CBPy** and **4-mCBPy** were measured to be 3.26 eV and 3.32 eV while the T_1 energies were measured to be 2.67 eV and 2.72 eV, respectively. The experimental S_1 and T_1 energies of **3-CBPy** and **4-mCBPy** are more stabilized than the DFT results (S_1 = 3.61; T_1 = 3.06 eV for **3-CBPy** and S_1 = 3.60; T_1 = 3.28 eV for **4-mCBPy**) calculated in the gas phase. **3-CBPy** exhibited slightly lower energy S_1 and T_1 states due to the extended conjugation. The ΔE_{ST} of **3-CBPy** and 4-**mCBPy** were calculated to be 0.59 eV and 0.60 eV. The S_1 energy of **3-CBPy** and **4-mCBPy** are slightly lower than the reported S_1 energies of **CBP** (3.45 eV) and **mCBP** (3.58 eV) as the donor-acceptor structure contributes to the stabilization of the S_1 state.[20] The T_1 energy of **3-CBPy** and **4-mCBPy** are similar to the reported T_1 energies of **CBP** (2.65 eV) and **mCBP** (2.75 eV). [20] The high triplet energies of **3-CBPy** and **4-mCBPy** should help to contain the triplet excitons within the emission layer.

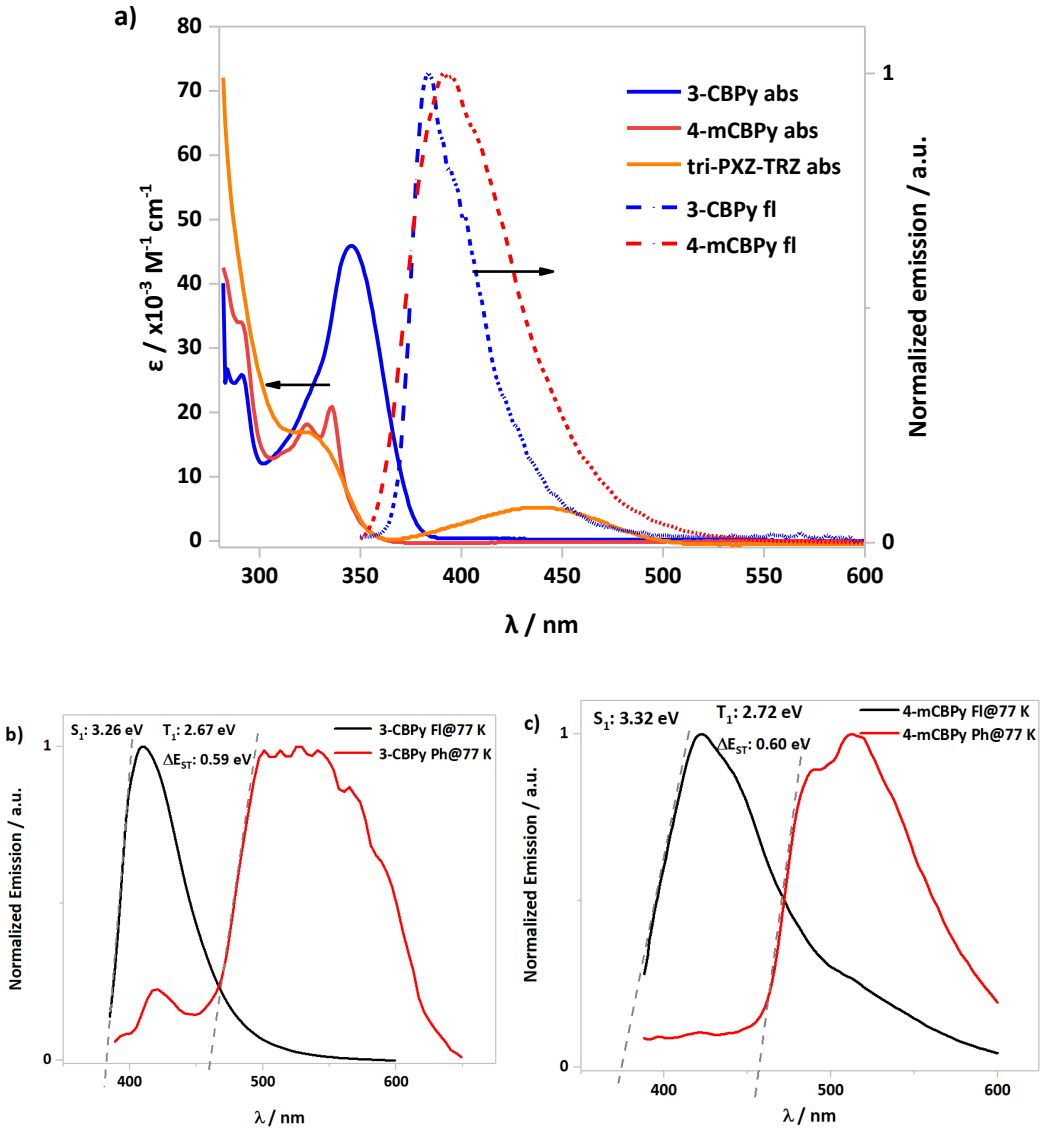

Figure **5.** (a) UV-vis absorption spectra of **3-CBPy**, **4-mCBPy** and **tri-PXZ-TRZ** and normalized photoluminescence spectra of **3-CBPy** and **4-mCBPy** in toluene (λ_{exc} = 340 nm). Fluorescence and phosphorescence spectra (by 10 ns and 2 ms) of (b) **3-CBPy** and (c) **4-mCBPy** neat film, measured at 77 K (λ_{exc} = 378 nm).

Table **1.** Summary of key optoelectronic properties of **3-CBPy** and **4-mCBPy**

Host	λ_{abs} (ε)[a] / nm (10^{-3} M^{-1} cm^{-1})	E_{opt} / eV	λ_{PL}[a] / nm	$S_1/T_1/\Delta E_{ST}$[b] / eV	HOMO/LUMO[c] / eV	$\Delta E_{H\text{-}L}$[d] / eV

3-CBPy	346 (46)/291 (26)	3.35	384	3.26/2.67/0.59	-5.75/-2.59	3.16
4-mCBPy	336 (21)/323 (17) 289 (34)	3.49	392	3.32/2.72/0.60	-5.80/-2.70	3.10

[a] Measured in PhMe. [b] S_1 energy determined from the onset of the prompt fluorescence spectra at 77 K and the T_1 determined from the onset of the phosphorescence spectra at 77 K (after 2 ms). [c] E_{HOMO} = -(E_{ox}^{onset} vs Fc/Fc^+ + 4.8) eV, E_{LUMO} = -(E_{red}^{onset} vs Fc/Fc^+ + 4.8) eV.[37] [d] $\Delta E_{H-L} = |E_{LUMO}-E_{HOMO}|$.

To evaluate the energy transfer efficiency between each of the two hosts and the emitter, we measured the Φ_{PL} and time-resolved PL spectra of 50 nm thick thermally evaporated films of 7 wt% **tri-PXZ-TRZ** doped in **3-CBPy** and **4-mCBPy**. For comparison, 7 wt% **tri-PXZ-TRZ** doped film in **CBP** and **mCBP** were also prepared as these hosts had been employed in the previously reported OLEDs.[12] The Φ_{PL} of the **tri-PXZ-TRZ** in **4-mCBPy** film is 50% while in **3-CBPy** it was slightly lower at 45%. The corresponding Φ_{PL} values in **mCBP** and **CBP** are 47% and 40%, respectively. As shown in Figure **6a**, the emission of films of **tri-PXZ-TRZ** in both **3-CBPy** and **4-mCBPy** showed a single peak originating from the emitter, whereas the emission spectra of the **CBP** and **mCBP** films revealed emission from both the host (400 nm) and the emitter (420 nm). These results imply a much less efficient FRET process in **CBP** and **mCBP** compared to the bipyridine-based host films. As shown in Figure **6b**, the time-resolved PL decay traces of the films measured under vacuum exhibited both a nanosecond prompt component (τ_p) and a microsecond delayed component (τ_d) at room temperature. The PL decays exhibited similar prompt lifetimes in all four hosts, which are ca. 25 ns. The τ_d is slightly shorter in **3-CBPy** (3.7 μs) and **4-mCBPy** (4.0 μs) than in **CBP** (3.9 μs) and **mCBP** (5.0 μs). The prompt component of the photoluminescence quantum yield (Φ_F) and delayed component of the photoluminescence quantum yield (Φ_d) efficiencies of **tri-PXZ-TRZ** in

each of the hosts were calculated from the PL decays by integrating the transient PL signals from 0 to 0.5 μs as originating from the prompt fluorescence and integrating signals from 0.5 μs to 45 μs as delayed fluorescence. The kinetics parameters of **tri-PXZ-TRZ** in different hosts are summarized in Table **2**. The four films all exhibited a high reverse intersystem crossing rate constant (k_{rISC}) (~2 × 10^5 s^{-1}), and the **3-CBPy** and **4-mCBPy**-based films exhibited faster prompt fluorescence decay rate constants (k_p), delayed fluorescence decay rate constants (k_d) and radiative decay rate constants from singlet state (k_r^s) than **CBP**- and **mCBP**-based films. These results imply that in **3-CBPy** and **4-mCBPy** the excitons on **tri-PXZ-TRZ** can radiatively decay more quickly thereby avoiding triplet exciton accumulation which can negatively impact both device stability and efficiency roll-off.

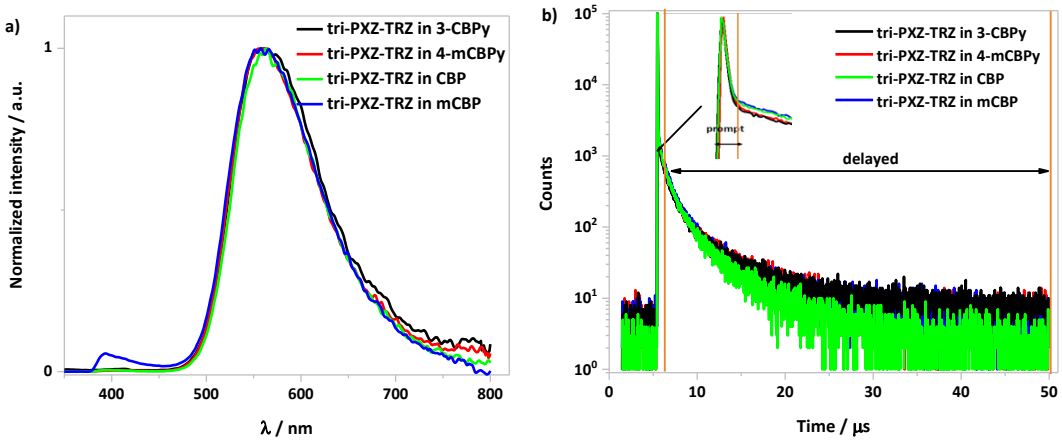

Figure **6.** (a) Photoluminescence spectra of 7 wt% doped **tri-PXZ-TRZ** in different hosts and (b) transit PL decay curves of 7 wt% doped **tri-PXZ-TRZ** in different hosts (λ_{exc} = 378 nm).

Table 2: Exciton lifetime and the kinetic constants of **tri-PXZ-TRZ** in different host materials

Host	τ_p [a] /ns	τ_d [b] /μs	Φ_{PL} [c] /%	Φ_p [d] /%	Φ_d [e] /%	k_p [f] / 10^{-7} s^{-1}	k_d [g] / 10^{-5} s^{-1}	k_r^{sh} / 10^{-7} s^{-1}	k_{ISC} [i] / 10^{-7} s^{-1}	k_{rISC} [j] / 10^{-5} s^{-1}	k_{nr}^T [k] / 10^{-5} s^{-1}
3-CBPy	19	3.7	45	22	23	5.26	2.70	1.16	4.10	3.62	1.20

4-mCBPy	20	4.0	50	28	22	5.10	2.50	1.43	3.67	2.72	1.73
CBP	26	3.9	40	20	20	3.85	2.56	0.77	3.08	3.20	1.92
mCBP	24	5.0	47	22	25	4.17	2.00	0.92	3.25	2.92	1.36

[a] Prompt emission lifetime. [b] Delayed emission lifetime. [c] Photoluminescence quantum yield. [d] Prompt component of Φ_{PL}. [e] Delayed component of Φ_{PL}. [f] Prompt fluorescence decay rate constant. [g] Delayed fluorescence decay rate constant. [h] Radiative decay rate constant from the singlet excited state. [i] Intersystem crossing rate constant. [j] Reverse intersystem crossing rate constant. [k] Non-radiative decay rate constant from the triplet excited state.

OLED characteristics

The suitably high T_1 energies **3-CBPy and 4-mCBPy** imply that the two hosts can confine the triplet excitons of the yellow emitter **tri-PXZ-TRZ**. We expected that the two bipyridine-containing hosts would also have ambipolar charge transport characteristics that would improve OLED performance. To test this, hole-only devices with the configuration of ITO/NPB (10 nm)/TCTA (5 nm)/Host (30 nm)/NPB (15 nm)/Al (100 nm) and electron-only devices with the configuration of ITO/TmPyPB (15 nm)/ Host (30 nm)/TmPyPB (15 nm)/LiF (1 nm)/Al (100 nm) were fabricated. As shown in Figure **7**, the devices with **3-CBPy** and **4-mCBPy** exhibit suppressed hole transport and largely enhanced electron transport compared to those with **CBP** and **mCBP**. These results point to an improved charge carrier balance in the **3-CBPy** and **4-mCBPy**-based devices.

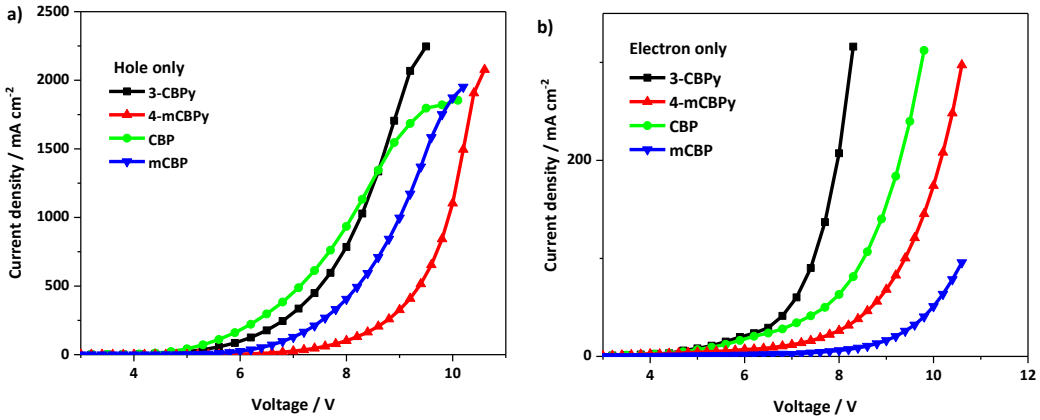

Figure **7.** Current density-voltage characteristics of (a) hole-only and (b) electron-only devices of the four hosts

Next, we fabricated yellow OLEDs with the following structure: ITO/NPB (30 nm)/TCTA (20 nm)/host (30 nm)/ PPT (5 nm)/TmPyPB (60 nm)/LiF (1 nm)/Al (100 nm), where host is as follows: Device A: **tri-PXZ-TRZ**:**3-CBPy** (7 wt%), Device B: **tri-PXZ-TRZ**:**4-mCBPy** (7 wt%), Device C: **tri-PXZ-TRZ**:**CBP** (7 wt%), Device D: **tri-PXZ-TRZ**:m**CBP** (7 wt%). In the devices, *N,N'*-bis-(1-naphthalenyl)-*N,N'*-bis-phenyl-(1,1'-biphenyl)-4,4'-diamine (NPB) was used as the hole injection layer, 4,4',4''-tris(carbazol-9-yl)triphenylamine (TCTA) was used as the hole-transporting layer, 2,8-bis(diphenylphosphoryl)dibenzo[b,d]thiophene (PPT) was use as a hole blocking layer, and 3,3'-[5'-[3-(3-pyridinyl)phenyl][1,1':3',1''-terphenyl]-3,3''-diyl]bispyridine (TmPyPB) was used as a combined electron-transporting and injection layer. Figure **8a** shows a proposed energy level diagram for our devices, indicating that the chosen stack architecture is likely to provide efficient injection and confinement of charge carriers to the emission layer (EML), and Figure **8e** shows the molecular structures of materials used in devices. A doping concentration of 7 wt% was applied across all OLEDs in this study, which is similar to the concentration adopted in the original report (6 wt%).[13]

The J-V-L characteristics of the fabricated yellow OLEDs are shown in Figure **8b** and the performance of the four devices are summarized in Table **3.** The devices based on **3-CBPy** (Device A) and **4-mCBPy** (Device B) exhibited relatively lower turn-on voltages (~ 2.5 V) compared to Device D based on **mCBP** (~ 3 V). Device C using **CBP** also exhibited low turn-on voltage of 2.5 V; however, this device showed poor stability at high voltage as the luminance plateaued and the current density increased dramatically. Figure **8c** shows the external quantum efficiency (EQE) curves as a function of luminance. An EQE_{max} of 19.4% was obtained at a luminance of 3 cd m^{-2} for Device B based on **4-mCBPy** while the EQE_{max} for Device D based on **mCBP** was lower at 16.7% and occurred at a luminance of less than 1 cd m^{-2}. The EQE_{max} for Device A based on **3-CBPy** was 15.6% at a luminance 2 cd m^{-2} while the Device C based on **CBP** showed very low EQE at low brightness due to relatively large leakage current but an EQE_{max} of 14.8 % at a luminance 300 cd m^{-2}. The low EQE of Device C could be ascribed in part to the unbalanced charge transport in **CBP** which leads to poor exciton utilization. Impressively, at a brightness of 10,000 cd m^{-2}, the EQE for Device B remained high at 16.0%, showing very low roll-off of 18%, while for Devices A, C and D, the $EQE_{10,000}$ dropped to 9.9%, 11.0%, and 11.5%, respectively corresponding to 36%, 26%, and 31% roll-off, respectively. The **3-CBPy**-based Device A exhibited more severe efficiency roll-off, which might be attributed to the fast k_{ISC} of **tri-PXZ-TRZ** in **3-CBPy** that leads to increased triplet exciton accumulation. The maximum brightness for Devices A and B both reached 86 000 cd m^{-2}, much higher than that achieved for Devices C and D, where maximum brightness reached only 38 000 cd m^{-2}. The electroluminescence (EL) spectrum of Device A (λ_{EL} = 561 nm) was slightly red-shifted relative to those of Devices B, C, and D (λ_{EL} – 555, 554, and 554 nm, respectively, Figure

8d). The high EQE and small efficiency roll-off make the device based on **tri-PXZ-TRZ/4-mCBPy** among the best yellow OLEDs employing TADF emitters (Table **S2**). We attribute the superior electroluminescence performance of the **4-mCBPy**-based Device B to a combination of improved electron transport, which results in better charge balance within the EML, and the highly efficient energy transfer from host to emitter. For the **3-CBPy**-based Device A, as the Φ_{PL} of the emitter in **3-CBPy** is lower than in **4-mCBPy** or **mCBP**, the EQE_{max} of Device A is also slightly lower than Devices B (**4-mCBPy**) and D (**mCBP**).

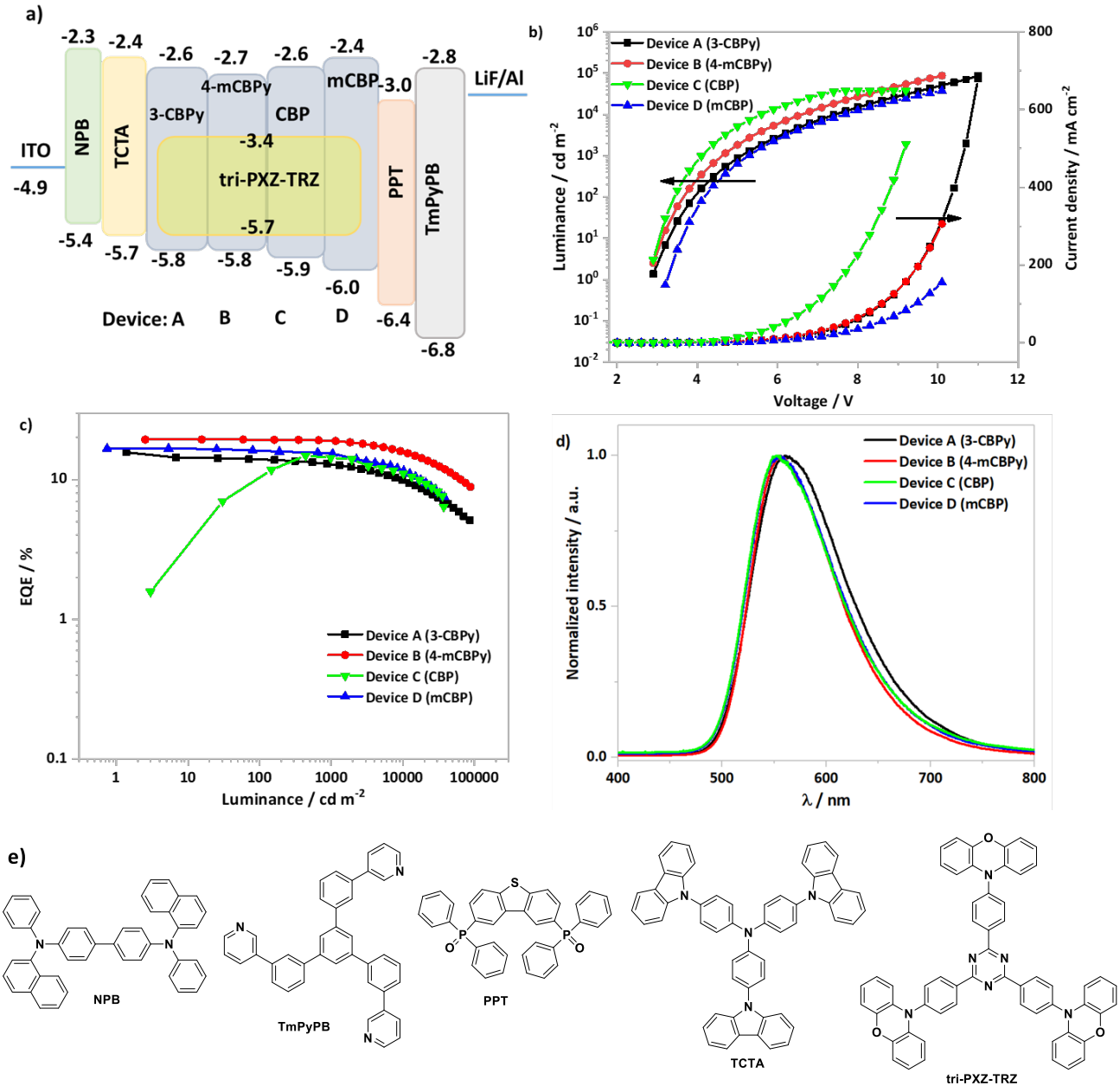

Figure **8**. Optimized OLED devices based on **3-CBPy** (Device A), **4-mCBPy** (Device B), **CBP** (Device C), and m**CBP** (Device D). (a) Energy level diagram of the device structure, (b) Current density-voltage-luminance characteristics, (c) EQE-luminance characteristics, (d) electroluminescence spectra, (e) molecular structure of materials used in devices.

Table **3**. Summary of OLEDs performance based on **3-CBPy** (Device A), **4-mCBPy** (Device B), **CBP** (Device C), and **mCBP** (Device D)

Devices	**V_{on} / V**	**λ_{EL} / nm**	**CIE @ 8 V**	**EQE_{max}/EQE_{1000} /EQE_{10000}/ %**	**Roll-off @ 1000 /10,000 cd m^{-2} / %**	**CE_{max} / cd/A**	**Lum_{max} / cd m^{-2}**
Device A	2.5	561	(0.46, 0.52)	15.6/12.7/9.9	19/36	48.2	86 796
Device B	2.5	555	(0.44, 0.53)	19.4/18.9/16.0	2/18	63.4	87 886
Device C	2.5	554	(0.44, 0.54)	14.8/13.9/11.0	6/26	43.0	37 288
Device D	3.0	554	(0.44, 0.53)	16.7/15.3/11.5	8/31	54.3	37 952

Molecular orientation of the emitter in the different hosts

A key parameter for achieving OLEDs with high EQE is the molecular orientation of the emitter transition dipole moment.[21] Perfect horizonal alignment of the transition dipoles with respect to the substrate can lead to a 50% increase in EQE compared to a sample with an isotropic orientation of dipoles.[21b] It would then be interesting to verify whether this factor played a significant role in the high EQE achieved for Devices A and B in this study. Thus, we investigated the dipole orientation of **tri-PXZ-TRZ** in thin films (thickness, ~47 nm) of the four different hosts (Film A: **tri-PXZ-TRZ**:**3-CBPy**; Film B: **tri-PXZ-TRZ**:**4-mCBPy**; Film C: **tri-PXZ-TRZ**:**CBP**; Film D: **tri-PXZ-TRZ**:**mCBP**), using angle-resolved photoluminescence spectroscopy.[22] The resulting anisotropy factor *a* provides information about the relative amounts of vertical and horizontal dipoles in the film ($a = 0.33$ would correspond to perfectly isotropic orientation, $a < 0.33$ to preferentially horizontal orientation; see Supporting Information for details). As shown in Figure **9**, **tri-PXZ-TRZ** showed preferential horizontal orientation and similar fractions of horizontal

dipoles in both **CBP** and **3-CBPy**, namely a = 0.25 and a = 0.24, respectively. The emitter orientation was slightly less favorable in terms of outcoupling for **mCBP**, but it was still preferentially horizontal (a = 0.27). Interestingly, the emitters exhibited a preferentially vertical orientation in **4-mCBPy**, with a = 0.49. Based on the orientation factor alone, it would be therefore expected that a device based on **4-mCBPy** would have a lower EQE than the other devices. However, the lower outcoupling efficiency is clearly outweighed by an enhancement of charge carrier balance for the **4-mCBPy** based OLED with respect to OLEDs using the other hosts. Therefore, the results of the orientation measurement confirm the improved electronic properties of this material and better energy transfer from host to emitter, as discussed in the previous section.

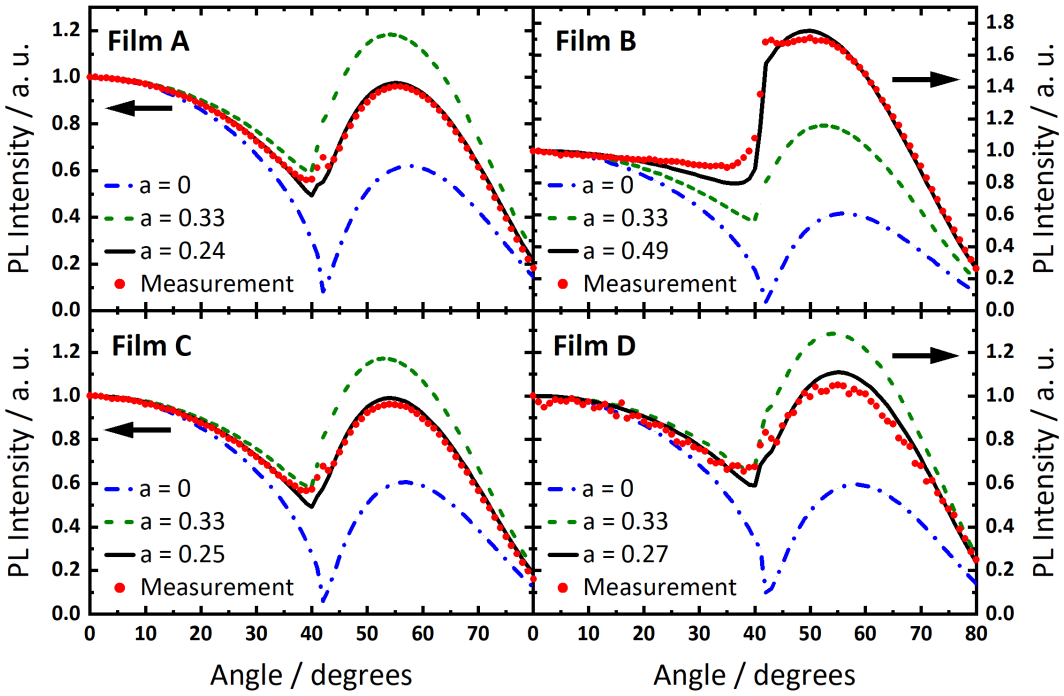

Figure **9**. Angular dependence of the photoluminescence (PL) intensity at the peak emission wavelength of films using **3-CBPy** (Film A), **4-mCBPy** (Film B), **CBP** (Film C), and **mCBP** (Film D) as host material. Red dots show the experimental data. The other curves represent the simulated intensity for a perfect horizontal alignment of emitters (blue dash-dotted line), for an isotropic

orientation (green dashed line), and for the best fit to the experimental data (black solid line). The corresponding anisotropy factors *a* for each curve are indicated in the legend of each panel. All data sets were normalized to the intensity at 0° of the corresponding curves.

Conclusions

This study demonstrates the potential of the bipyridine core as an effective acceptor an ambipolar host materials. Two bipolar host materials **3-CBPy** and **4-mCBPy** containing n-type carbazoles and p-type bipyridine moieties were synthesized and characterized in detail. Both materials possessed high singlet energy and triplet energies, and suitable HOMO and LUMO levels, that made them ideal hosts for yellow TADF-based OLEDs. Indeed, the materials enabled OLEDs with enhanced EQE and reduced efficiency roll-off when paired with a yellow TADF emitter. In particular, the device based on **4-mCBPy** exhibited a low turn-on voltage of 2.5 V along with an EQE_{max} of 19.4 %. This device also showed dramatically reduced efficiency roll-off; at a luminance of 10,000 cd m^{-2} its EQE remained at 16.0%.

Acknowledgements

We are grateful to the Engineering and Physical Sciences Research Council (EPSRC) for support from grants EP/P010482/1 and EP/R035164/1, and to EPSRC NSF-CBET lead agency agreement (EP/R010595/1, 1706207). Dongyang Chen thanks the China Scholarship Council (201603780001). P. Rajamalli acknowledges support from a Marie Skłodowska-Curie Individual Fellowship (MCIF; No. 749557).

Supporting Information

Experimental details, NMR spectra, HPLC traces, elemental analyses CIFs of the crystal structures (CCDC 1937093-1937094), details of theoretical calculations, photophysical and thermal properties, details concerning molecular orientation measurements are available in supporting information.

Graphical Abstract

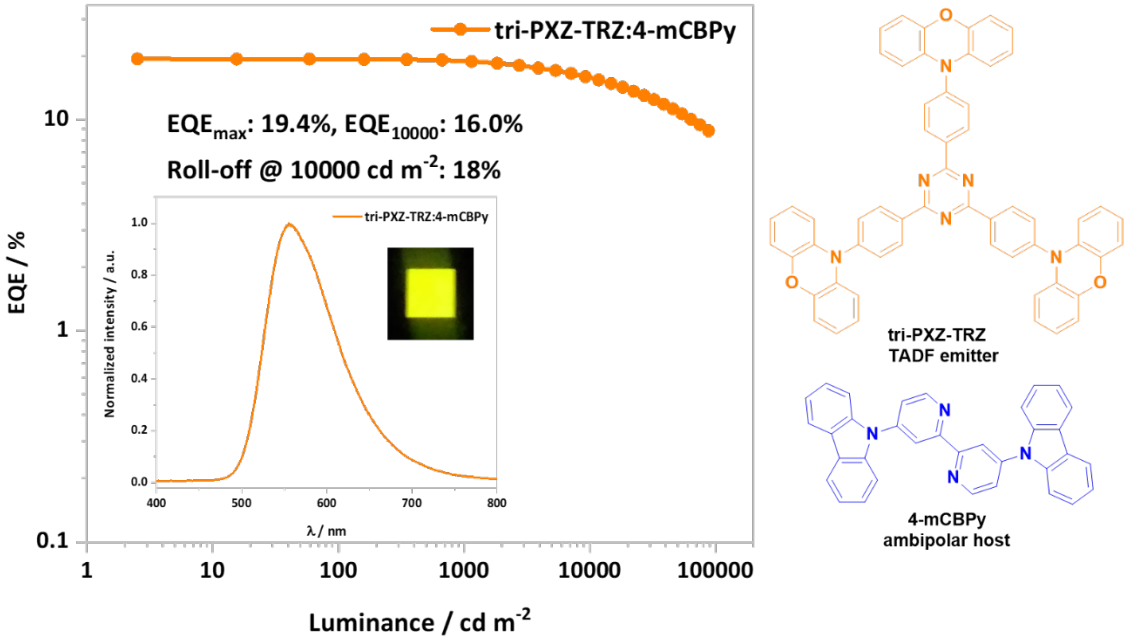

Summary

This work reveals how the rational design of host materials can significantly improve the performance of TADF-based OLEDs. We report two ambipolar host materials for use with a yellow TADF emitter and compared the properties with commercial host materials. The OLEDs device based on our host material shows not only near record maximum efficiencies (EQE_{max} = 19.4%), but also the lowest efficiency roll-off of any yellow TADF OLED, with EQE at 10,000 cd m^{-2} of 16%.

References

[1] a) H. Uoyama, K. Goushi, K. Shizu, H. Nomura, C. Adachi, *Nature* **2012**, *492*, 234; b) M. Y. Wong, E. Zysman-Colman, *Adv Mater* **2017**, *29*, 1605444; c) Y. Liu, C. Li, Z. Ren, S. Yan, M. R. Bryce, *Nat. Rev. Mater.* **2018**, *3*, 18020; d) Z. Yang, Z. Mao, Z. Xie, Y. Zhang, S. Liu, J. Zhao, J. Xu, Z. Chi, M. P. Aldred, *Chem. Soc. Rev.* **2017**, *46*, 915.

[2] F. B. Dias, T. J. Penfold, A. P. Monkman, *Methods Appl Fluoresc* **2017**, *5*, 012001.

[3] X. Liang, Z. L. Tu, Y. X. Zheng, *Chemistry* **2019**, *25*, 5623.

[4] a) H. Huang, Y. Wang, B. Wang, S. Zhuang, B. Pan, X. Yang, L. Wang, C. Yang, *J. Mater. Chem. C* **2013**, *1*; b) H. H. Chou, C. H. Cheng, *Adv Mater* **2010**, *22*, 2468.

[5] a) J. Li, D. Ding, Y. Tao, Y. Wei, R. Chen, L. Xie, W. Huang, H. Xu, *Adv. Mater.* **2016**, *28*, 3122; b) C.-C. Lin, M.-J. Huang, M.-J. Chiu, M.-P. Huang, C.-C. Chang, C.-Y. Liao, K.-M. Chiang, Y.-J. Shiau, T.-Y. Chou, L.-K. Chu, H.-W. Lin, C.-H. Cheng, *Chem. Mater.* **2017**, *29*, 1527.

[6] Y. Tao, C. Yang, J. Qin, *Chem Soc Rev* **2011**, *40*, 2943.

[7] T. Chatterjee, K.-T. Wong, *Adv. Optical Mater.* **2019**, *7*, 1800565.

[8] a) W. Li, J. Li, D. Liu, F. Wang, S. Zhang, *J. Mater. Chem. C* **2015**, *3*, 12529; b) J. S. Kang, T. R. Hong, H. J. Kim, Y. H. Son, R. Lampande, B. Y. Kang, C. Lee, J.-K. Bin, B. S. Lee, J. H. Yang, J. Kim, S. Park, M. J. Cho, J. H. Kwon, D. H. Choi, *J. Mater. Chem. C* **2016**, *4*, 4512; c) K. Masui, H. Nakanotani, C. Adachi, *Org. Electron.* **2013**, *14*, 2721; d) K. Gao, K. Liu, X.-L. Li, X. Cai, D. Chen, Z. Xu, Z. He, B. Li, Z. Qiao, D. Chen, Y. Cao, S.-J. Su, *J. Mater. Chem. C* **2017**, *5*, 10406; e) L.-S. Cui, S.-B. Ruan, F. Bencheikh, R. Nagata, L. Zhang, K. Inada, H. Nakanotani, L.-S. Liao, C. Adachi, *Nature Communications* **2017**, *8*, 2250.

[9] a) L.-S. Cui, J. U. Kim, H. Nomura, H. Nakanotani, C. Adachi, *Angew. Chem. Int. Ed.* **2016**, *55*, 6864; b) W. Li, J. Li, D. Liu, D. Li, F. Wang, *ACS Appl Mater Interfaces* **2016**, *8*, 21497.

[10] a) Y. Watanabe, H. Sasabe, D. Yokoyama, T. Beppu, H. Katagiri, J. Kido, *J. Mater. Chem. C* **2016**, *4*, 3699; b) T. Chatterjee, W.-Y. Hung, W.-F. Tang, H.-F. Chen, K.-T. Wong, *Org. Electron.* **2017**, *50*, 204; c) W.-Y. Hung, T.-C. Wang, H.-C. Chiu, H.-F. Chen, K.-T. Wong, *Phys. Chem. Chem. Phys.* **2010**, *12*, 10685.

[11] a) Y. Tao, Q. Wang, C. Yang, Q. Wang, Z. Zhang, T. Zou, J. Qin, D. Ma, *Angew Chem Int Ed Engl* **2008**, *47*, 8104; b) W. Song, L. Shi, L. Gao, P. Hu, H. Mu, Z. Xia, J. Huang, J. Su, *ACS Appl Mater Interfaces* **2018**, *10*, 5714; c) C. W. Lee, J. Y. Lee, *Chem. Commun.* **2013**, *49*, 1446; d) C. Tang, R. Bi, Y. Tao, F. Wang, X. Cao, S. Wang, T. Jiang, C. Zhong, H. Zhang, W. Huang, *Chem. Commun.* **2015**, *51*, 1650.

[12] H. Tanaka, K. Shizu, H. Nakanotani, C. Adachi, *Chem. Mater.* **2013**, *25*, 3766.

[13] X.-L. Li, X. Cai, M. U. Ali, S.-J. Su, H. Meng, *J. Mater. Chem. C* **2019**, 10.1039/C9TC02383F.

[14] S. Tao, E. Ji, L. Shi, N. Liu, L. Xu, B. Dai, *Synthesis* **2017**, *49*, 5120.

[15] a) M. Nishio, *CrystEngComm* **2004**, *6*, 130; b) M. Nishio, Y. Umezawa, K. Honda, S. Tsuboyama, H. Suezawa, *CrystEngComm* **2009**, *11*, 1757.

[16] P. Schrögel, N. Langer, C. Schildknecht, G. Wagenblast, C. Lennartz, P. Strohriegl, *Org. Electron.* **2011**, *12*, 2047.

[17] a) C. Adamo, V. Barone, *J. Chem. Phys.* **1999**, *110*, 6158; b) J. A. Pople, J. S. Binkley, R. Seeger, *Int. J. Quant. Chem. Symp.* **1976**, *10*, 1.

[18] R. T. White, E. S. Thibau, Z.-H. Lu, *Sci. Rep.* **2016**, *6*, 21109.

[19] G. Gritzner, J. Kuta, *Pure Appl. Chem.*, **1984**,56, 461.

[20] S. A. Bagnich, A. Rudnick, P. Schroegel, P. Strohriegl, A. Köhler, *Phil. Trans. Royal Soc., A* **2015**, *373*, 20140446.

[21] a) Y. Watanabe, H. Sasabe, J. Kido, *Bull. Chem. Soc. Jpn.* **2019**, *92*, 716; b) K.-H. Kim, J.-J. Kim, *Adv. Mater.* **2018**, *30*, 1705600; c) T. D. Schmidt, T. Lampe, D. Sylvinson M. R, P. I. Djurovich, M. E. Thompson, W. Brütting, *Physical Review Applied* **2017**, *8*, 037001.

[22] A. Graf, P. Liehm, C. Murawski, S. Hofmann, K. Leo, M. C. Gather, *J. Mater. Chem. C* **2014**, *2*, 10298.